RESEARCH PAPER

Magnetohydrodynamic Boundary Layer Flow of Radiative Ternary-Hybrid Nanofluid Over a Variable Thickness Porous Surface with Variable Thermal Conductivity

Anjayya N Erla[1], Dr. G V V Jagannadha Rao[2], Dr. Shailendra D. Deo[3]

[1] Department of Mathematics, Kalinga University, Naya Raipur (CG), India - 492101.

[2] Department of Mathematics, Kalinga University, Naya Raipur (CG), India - 492101.

[3] Mahatma Gandhi College of Science, Gadchandur, Dist. Chandrapur (MS), India - 442908.

Received: 20th Feb, 2026 | **Revised:** 4th Mar, 2026 | **Accepted:** 25th Mar, 2026 | **Available Online:** 10th Apr, 2026

ABSTRACT

In the present scenario, trihybrid nanofluids (THNF) have emerged as a promising fluid to optimize thermal properties of systems. While previous studies have explored individual or binary nanoparticle dispersion under idealized thermal models, this research investigates the effect of thermal radiation (non-linear) and viscous dissipation on the flow and thermal characteristics of a tri-hybrid nanofluid (THNF) composed of TiO_2-Al_2O_3-MoS_2 spherical nanoparticles dispersed in kerosene oil, flowing through porous sheets of varying thicknesses. The present study introduces a novel combination of three distinct nanoparticles, leveraging their complementary thermal properties to enhance heat transfer (HT) in porous geometries. The effective dynamic viscosity and thermal conductivity (temperature-dependent) are modeled using Batchelor and Hamilton-Crosser models, respectively. The controlling dimensional equations are transmuted to non-dimensional ordinary differential equations (ODEs), using the similarity constraint and then solved using the bvp4c solver. A key novelty lies in the assessment of THNF behavior under coupled influences of porosity variation, slip boundary conditions, and non-linear radiative heat transfer. It simultaneously offers new insights into complex energy transport phenomena. This study's findings suggest that fluid velocity decreases with an increase in the magnetic and slip parameters, whereas the temperature rises with porosity and dissipation, respectively. It has been found that adding one unit to the porosity parameter (2.15 to 3.15) causes the magnitude of the Nusselt number (LNN) to drop by almost 4.87%, and adding one unit to the thermal conductivity parameter (2.45 to 3.45) causes it to drop by almost 14%. The skin friction coefficient (SFC) increases by approximately 0.645% as both parameters increase from 1.0 to 1.4.

Keywords: Variable thickness surface; Tri-hybrid nanofluid; Thermal radiation; Temperature-dependent thermal conductivity; Joule heating.

How to cite this article: Erla AN, Rao GVVJ, Deo SD. Magnetohydrodynamic Boundary Layer Flow of Radiative Ternary-Hybrid Nanofluid Over a Variable Thickness Porous Surface with Variable Thermal Conductivity. Int J Drug Deliv Technol. 2026;16(29s):936-945. DOI: 10.25258/ijddt.16.29s.117

Source of support: Nil.

Conflict of interest: The authors declare no conflict of interest.

1. Introduction

Nanoparticles have attracted researchers due to their unique thermal and chemical properties, which make them essential in a vast and multipurpose areas. Since their size ranges between 1-100 nanometers, they exhibit a high surface area to volume ratio,and this increases the interaction of these particles with base fluids. Owing to these properties, nanoparticles are exceptionally well-suited for integration into advanced materials, especially in systems that require efficient HT and mass transfer. In various thermal systems, it is necessary to carefully select the nanoparticles so as to determine the performance, applicability and stability. This study considers TiO_2, Al_2O_3 and MoS_2 as nanoparticles. A poor choice may lead to sedimentation, agglomeration or corrosion. Similarly, the base fluid and nanoparticles' compatibility are important points to be considered to ensure the stability and avoid phase separation or adverse interaction. While TiO_2 and Al_2O_3 are commonly chosen due to their high chemical stability and economic viability, MoS_2 offers significant advantages in terms of thermal enhancement and tribological performance, making it particularly useful in high-temperature and mechanical stress environments. Due to this, the present study considers

these nanoparticles for creating a tri-hybrid nanofluid.Choi [1] observed an improvement in thermal conductivity (TC) in conventional fluids by dispersing nanoparticles.Later, Xuan and Li [2] addressed important factors such as particle shape and dimension and proposed a theoretical model for TC. Sridhara and Satapathy [3] studied the impact of nanoparticles on optimizing the thermal properties of different oils. They summarized the work and developments on oil-based nanofluids. Tiwari and Das [4] studied the properties of nanofluid (NF) in a heated square cavity and used the SIM-PLE scheme to solve the changed equations. Shima et al. [5] analysed the impact of TC of dispersed nanomaterials on thermal properties of metal oxide nanofluid. They confirmed that the TC of nanofluids depends on the volume fraction of nanoparticles.Zahmatkesh et al. [6] also studied the impact of nanoparticle shape on the performance of thermal systems. It included convection regimes, reviewed the study over heat exchangers, boundary layer flows, peristaltic flows, cavity flows and impinging jets. Tang et al. [7] analysed the NF containing different-shaped nanoparticles and studied their behavior on the boiling transition.Researchers have continued exploring theHT properties of NF [8–9], as NF results in enhanced HT. The day-to-day use of NF in power generation and nuclear reactors motivates researchers to work on combining two types of nanoparticles in the base fluid. Thus, the concept of "hybrid nanofluid" came into existence. Hybrid nanofluids (HF) are reported to exhibit better TC than mono-nanofluids (MNF); they also possess better stability and a longer shelf life compared to MNF due to the synergistic effect between the different types of nanoparticles. Devi and Devi [10]first utilized experimental data on TC. They presented a theoretical model for HF along a stretching sheet and concluded that choosing appropriate nanoparticles results in a higher rate of HT for HF. Sheikholeslami [11] and Bhatti et al. [12] described the application of HF in the solar system and numerical simulation. They employed the Semi linearization approach to solve the transport equations. Gupta et al. [13] organized the numerical simulation for the variable viscosity-based HF model. The Legendre wavelet collocation technique solved the transmuted equations. Xia et al. [14] addressed the flow of HF across a slanted surface under the influence of non-linear convection and multiple slip conditions. Researchers have continued exploring the HT properties of HF [15–17].

Recently, the concept of “hybrid nanofluid" has been expanded by adding three various kindsof nanoparticles, and the new fluid is referred to as "ternary hybrid nanofluid’’(THNF).This enables a synergistic enhancement in heat transfer, stability, and energy efficiency. In the industrial field, these types of fluids have shown improved performance by providing faster thermal response and better heat removal tendency. Sahoo and Kumar [18] performed an experiment on the Al_2O_3-CuO-TiO_2 water-based THNF. The researchers hypothesized the presence of a compact particle with a concentration between 0.01% and 0.1% at temperatures between 350°Cand 500°C. They determined that the deviation was 1.5%, indicating a significant difference from the expected value. Arif and colleagues [19] introduced a theoretical framework to describe the movement of water-based THNF across channels. The researchers are able to determine the precise solution to the flow equation using Laplace and Fourier transforms. Manjunatha et al. [20] presented a theoretical model for TNHF across a convective-heated sheet. The authors examined the comparison between NF, HF, and THNF. Ramzan et al. [21] outlined the simulation for turbulent HT across a spinning surface. Their discussion focused on the consequence of the Hall current effect and the porosity effect on the energy profile.

The study of boundary layers is crucial to its vast application in engineering; Sakiadis [22] was the pioneer to communicate this concept to the human race by learning about the boundary layer behaviour on a moving surface. Whaed et al. [23] formulated a model for stretching sheets with variable thickness. They investigated the effects of nonlinear Brownian motion flow on nanofluids. Furthermore, Khan et al. [24] considered the bio-convection slip flow of nanofluid over a porous stretching sheet. They included gyrotactic microorganisms in their study. Their study disclosed that the Schmidt number enhances the concentration of microorganisms and nanoparticles for the specific scenario considered in their problem. Alqarni et al. [25] analysed the stagnation point flow of a Casson fluid over a twisted cylinder in the vicinity of MHD effect. Recently, a study was presented by Khan et al. [26] in which the HT of Jeffery nanofluid was taken into account. This analysis was done to study the stress relaxation in non-Newtonian fluids over a stretched surface in presence of MHD and slip effects.Yaseen et al. [27] extended the work on hybrid nanofluids and

investigated the effects of viscous dissipation and heat source/sink. According to their study, increasing SiO_2 particles from 1% to 5% resulted in a 15% increase in the heat transfer coefficient. Recently, the variable characteristics of fluids have attracted much attention from investigators. Mandal and Pal [28] showed how the changing thermal conductivity and viscosity of HF (Ag-MoS_2/Water) affected a surface in Riga that was getting smaller and smaller. Eid and Nafe [29] demonstrated how the use of MHD alters the flow of HF along porous sheets due to the influence of thermal conductivity. They detected the various parameters against the velocity and thermal profiles.

Most of the existing nanofluid workis limited to mono or binary combinations with idealized conditions, often disregarding the complex interactions and enhanced capabilities of ternary hybrid nanofluids, with real-world phenomena such as porous media, slip and nonlinear radiation. This research fills the gap by assuming that THNF is composed of TiO_2-Al_2O_3-MoS_2 nanoparticles in kerosene oil in the vicinity of temperature-dependent thermophysical characteristics with the aid of Batchelor and Hamilton-Crosser formulations. The authors studied the flow of an MHD ternary hybrid nanofluid on a porous stretching sheet, exposed to nonlinear thermal radiation conditions, due to industrial uses. It is appropriate for simulating thermal conditions in which the density variation with respect to temperature is significant, such as solar collectors.Moreover, the novelty of the work can be visualized from Table 5. The following are some other significant aspects to pay attentionto in this paper:

- This study inspects the flow of ternary nanofluid over porous variable thickness sheets.
- Simulating the flow behavior influenced by magnetic fields, porosity, and nonlinear thermal radiation factors.
- The thermal conductivity of THNF is variableusing Batchelor and Hamilton-Crosser models.
- Analyzing theSFC and LNN profiles in relation to various physical parameters by contour plot.

2. Problem assumptions and formulation

Consider a plate placed in $xy-$plane of a rectangular coordinate system as shown in Figure 1. Assume a time-independent, viscous, two-dimensional flow of tri-hybrid nanofluid across the continuously moving surface. Considering that the surface is sustainably thin, the present study operates under the following assumptions:

- The plate's surface is intended to be non-flat (i.e., variable thickness) and porous, which is described as $y = D(x+c)^{\frac{1-n}{2}}$, varying with distance from the origin.
- The fluid flow is considered to be convective, and a magnetic field is provided perpendicular to the wall. Consequently, the conservation of momentumequation is formulated by including the applied magnetic field and surface porosity.
- The flow resulting from the elongation of the plate and the influence of velocity slip are both accounted for SFC and LNN.
- The energy equation is formulated based on Fourier's law. In the present investigation, the heating process is facilitated by Joule heating, nonlinear thermal radiation source and dissipation.
- Here, we disperse TiO_2, Al_2O_3, and MoS_2nanoparticles in kerosene oil, the base fluid, to create a tri-hybrid nanofluid (TiO_2-Al_2O_3-MoS_2/kerosene oil). Table 1 describes the thermophysical properties of the THNF component.
- Thermal conductivity is taken as temperature-dependent.

According to the assumptions, the equations for regulating fluid flow are formulated as[27-30]

$$U_x + U_y = 0, \tag{1}$$

$$UU_x + VU_y = \frac{\mu_{Tf}}{\rho_{Tf}}U_{yy} - \frac{\sigma_{Tf}}{\rho_{Tf}}B_0^2 U - \frac{\mu_{Tf}}{\rho_{Tf}}\frac{U}{K^*} + \frac{g}{\rho_{Tf}}\left[\left(\rho\beta_o\right)_{Tf}\left(T - T_\infty\right)\right], \tag{2}$$

$$\left(\rho C_P\right)_{Tf}\left[\left(UT_x + VT_y\right) + \right] = \frac{\partial}{\partial y}\left(K_{Tf}(T)T_y\right) + \sigma_{Tf}B_0^2U^2 + \mu_{Tf}(U_y^2) + \frac{16\sigma^*}{3k^*}\frac{\partial}{\partial y}\left(T^3T_y\right) \tag{3}$$

Along the following boundary constraints [29]

$$U(x,y) = U_s + \gamma\left(U_y\right), V(x,y) = 0, T = T_s, \quad y = D(x+c)^{\frac{1-n}{2}},$$
$$U \to 0,\ T \to T_\infty \quad y \to \infty. \tag{4}$$

Here,the velocity components along x- and y- axes are Uand V, K^* permeability of the medium, B_0 magnetic field strength, T temperature, T_s wall temperature, T_∞ ambient temperature, K thermal conductivity, μ dynamic viscosity, σ electrical

conductivity, C_P heat capacitance, and β_0 thermal expansion, and ρ density. The R.H.S terms in equation (2) are the magnetic, porosity and convection effects.

The TC of the fluid is defined as [13]

$$K_{Tf}(T)=\frac{K_{Tf}}{K_f}K_f(T) \tag{5}$$

where $K_f(T)=K_\infty(1+\varepsilon\theta)$.

Before solving the governing equations (1-3), it is necessary to reduce them to non-dimensional ODEs; this is accomplished via the similarity transformations listed below [27,30].

$$\left.\begin{aligned}\psi&=\left(\left(\frac{2}{n+1}\right)\upsilon_f U_0(x+c)^{(n+1)}g(\xi)\right)^{0.5},\ \xi=\left(\frac{n+1}{2}\frac{U_0}{\upsilon_f}(x+c)^{n-1}\right)^{0.5}y,\ U=U_0(x+c)^n g'(\xi)\\ V&=-\left(\frac{n+1}{2}\upsilon_f U_0(x+c)^{n-1}\right)^{0.5}\left[g(\xi)+\xi\frac{n-1}{n+1}g'(\xi)\right],\ \Theta(\xi)=\frac{T-T_S}{T_S-T_\infty}\end{aligned}\right\} \tag{6}$$

After applying (6), Eq. (1) is satisfied identically, and Eqs. (2–3) along with (4) reduce to the following forms:

$$\varpi_1\left(g'''-\beta\chi g'\right)+\varpi_2\left(gg''-(2-\beta)g'^2\right)-\beta M\varpi_3 g'+\varpi_4\varsigma\Theta=0 \tag{7}$$

$$\varpi_6\left[(1+\varepsilon\Theta)\Theta''+\varepsilon\Theta'^2\right]+R_d\left(1+\Theta(\theta_s-1)\right)^2\left[\Theta''+(\theta_s-1)\left[\Theta\Theta''+3\Theta'^2\right]\right]+\varpi_1 Ec\,\mathrm{Pr}\,g''^2+\frac{2}{m+1}\varpi_3 MEc\,\mathrm{Pr}\,g'^2+\varpi_5\,\mathrm{Pr}\,g\Theta'=0 \tag{8}$$

with the ensuing boundary conditions

$$\left.\begin{aligned}&g(\delta)=\delta\frac{(1-n)}{(1+n)},\ g'(\delta)=1+\gamma g''(\delta),\ \Theta(\delta)=1 \ \ at\ \delta\left(=D\sqrt{\frac{U_0(n+1)}{2\upsilon_f}}\right)\\ &g'(\delta)=0,\ \Theta(\delta)=0 \qquad\qquad as\ \delta\to\infty\end{aligned}\right\} \tag{9}$$

Now, to convert the domain of integration from $[\delta,\infty)$ to $[0,\infty)$, invoke the following transformation.

$$\left.\begin{aligned}g(\xi)&=f(\eta)\left(=g(\xi-\delta)\right)\ and\\ \Theta(\xi)&=\theta(\eta)\left(=\Theta(\xi-\delta)\right)\end{aligned}\right\} \tag{10}$$

Using (10), the following form of Eqs. (7-8) and (9) are obtained

$$\varpi_1\left(f'''-\frac{2n}{1+n}\chi f'\right)+\varpi_2\left(ff''-\left(\frac{2}{1+n}\right)f'^2\right)-\frac{2n}{1+n}M\varpi_3 f'+\varpi_4\varsigma\theta=0 \tag{11}$$

$$\varpi_6\left[(1+\varepsilon\theta)\theta''+\varepsilon\theta'^2\right]+R_d\left(1+\theta(\theta_s-1)\right)^2\left[\theta''+(\theta_s-1)\left[\theta\theta''+3\theta'^2\right]\right]+\varpi_1 Ec\,\mathrm{Pr}\,f''^2+f'^2\frac{2}{n+1}MEc\,\mathrm{Pr}\,\varpi_3+f\theta'\,\mathrm{Pr}\,\varpi_5= \tag{12}$$

with

$$\left.\begin{aligned}&f(0)=\delta\left(\frac{1-n}{1+n}\right),\ f'(0)=1+\omega f''(0),\ \theta(0)=1\\ &f'(\infty)=0,\ \theta(\infty)=0\end{aligned}\right\} \tag{13}$$

Here, the symbols appearing in the above equations and boundary conditions are defined as $M\left(=\frac{B_0^2\sigma_f}{\rho_f u_\infty}\right)$ is the magnetic parameter, $Gr_x\left(=\frac{g_0\beta_f\left[\left(T_S-T_\infty\right)\right](x+b)^3}{\upsilon_f^2}\right)$ local Grashof number, $\chi\left(=\frac{Gr_x}{\mathrm{Re}_x^2}\right)$ mixed convection parameter, $\mathrm{Pr}\left(=\frac{\upsilon_f}{\alpha_f}\right)$, Prandtl number, $\lambda^*\left(=\frac{\upsilon_f}{K^*\left(U_0(x+b)^{m-1}\right)}\right)$ permeability of porous media, $\mathrm{Re}_x\left(=\frac{U_s(x+b)}{\upsilon_f}\right)$ local Reynolds number, $Rd\left(=\frac{16\sigma^*T_\infty^3}{3k^*k_f}\right)$ radiation parameter, $\varepsilon\left(=\frac{\left(k_s-k_\infty\right)}{k_\infty}\right)$ variable thermal conductivity, $\omega\left(=\sqrt{\frac{U_0(m+1)}{2\upsilon_f}}\right)$ velocity slip parameter. $\theta_s\left(=\frac{\left(T_s-T_\infty\right)}{T_\infty}\right)$ thermal ratio factor, $Ec=\frac{U_S}{\left(T_S-T_\infty\right)\left(c_p\right)_f}$ And, $\varpi_1\left(=\frac{\mu_{Tf}}{\mu_f}\right)$, $\varpi_2\left(=\frac{\rho_{Tf}}{\rho_f}\right)$, $\varpi_3\left(=\frac{\sigma_{Tf}}{\sigma_f}\right)$, $\varpi_4\left(=\frac{(\rho\beta)_{Tf}}{(\rho\beta)_f}\right)$, $\varpi_5\left(=\frac{\left(\rho C_p\right)_{Tf}}{\left(\rho C_p\right)_f}\right)$, $\varpi_6\left(=\frac{K_{Tf}}{K_f}\right)$ are the ratio of the thermophysical properties of THNF to base fluids.

The correlations to compute $\varpi_i, 0 \le i \le 6$ are provided in Table 2.

The surface drag and local Nusselt number are defined as[31-32]

(i) SFC: $$C_f = \left[\frac{\mu_{Tf}}{\rho_f U_s} U_y\right]_{y=D(x+c)^{\frac{1-n}{2}}} \quad (14)$$

(ii) LNN:

$$Nu = -\frac{(x+c)}{k_\infty (T_s - T_\infty)}\left[k_{Tf}(T)T_y + \frac{4\sigma^*}{3k^*}\frac{\partial T^4}{\partial y}\right]_{y=D(x+c)^{\frac{1-n}{2}}} \quad (15)$$

Using (6) and (10), the following dimension-free form of SFC and LNN is

$$Cf_x^* = C_f \,\mathrm{Re}_x^{1/2} = \varpi_1 \left(\frac{2}{n+1}\right)^{\frac{-1}{2}} f''(0) \quad (16)$$

$$Nu_x^* = Nu\,\mathrm{Re}_x^{-1/2} = -\left[\varpi_6 (1+\varepsilon\theta) + R_d (1+(\theta_s - 1))^3\, \theta(0)\right]\theta'(0) \quad (17)$$

3. Solution Methodology

In the past decades, numerous studies have been published on the bvp4c solver; Kierzenka and Shampine [33] were the first to solve equations using the bvp4c solver. In this approach, firstly,the coupled equations are transmuted to a set of first-order equations, and this is done by using these variables:

$$f = t_1, \quad f' = t_2, f'' = t_3, \theta = t_4, \quad \theta' = t_5, \quad (18)$$

Employing (18), the Eqs. (11) and (12) are rewritten in the following form:

$$tt_1 = -\frac{\varpi_2}{\varpi_1}\left(t_1 * t_3 - (2-\beta) * t_2^2\right) + \frac{\varpi_2}{\varpi_1} * \beta * M * \varpi_3 * t_2 - \frac{\varpi_2}{\varpi_1} * \varpi_4 * \xi * t_4 + \beta * \lambda^* * t_2$$

$$tt_2 = \frac{-\varpi_6 * \varepsilon * t_5 * t_5 - 3R_d\left(1 + t_4 * (\theta_s - 1)\right)^2 (\theta_s - 1) * t_5 * t_5 - \varpi_1 * Ec * \Pr * t_3 * t_3 + \beta * \varpi_3 * M * Ec * \Pr * t_2 * t_2 + \varpi_5 * \Pr * t_1 * t_5}{\left(\varpi_6 * (1 + \varepsilon * t_4) + Rd * (1 + t_4 * (\theta_s - 1))^3\right)} \quad (19)$$

with

$$\left.\begin{aligned} t_2(a) = 1 + \omega * t_3(a), t_1(a) = \delta\left(\frac{1-n}{1+n}\right)\left[1 + \omega * t_3(a)\right], t_4(a) = 1 \\ t_2(b) = 1, t_5(b) = 1 \end{aligned}\right\} \quad (20)$$

The bvp4c solver is accessed by the syntax described below

"sol = bvp4c(@odeBVP, @odeBC, solinit, options)''

Now, in order to confirm the approach that was followed, the authors verified their findings by comparing them to those of published research by Fang et al. [34] and Elbashbeshy et al. [35]. The results are in good conciliation; see Table 3.

4. Findings and analysis

This section discusses the influence of dimensionless factors like magnetic parameter (M), porosity parameter (λ^*), radiation parameter (R_d), dissipation parameter (Ec), thermal ratio parameter (θ_s), slip parameter (ω) and variable thermal conductivity (ε)on the velocity and thermal profile of THNF (TiO_2-Al_2O_3-MoS_2/kerosene oil).

Effect of porosity parameter

In porous media applications such as packed bed reactors, geothermal reservoirs, or catalytic converters, the porosity parameter directly influences flow resistance and thermal management.Figures 2 and 3 are sketched to depict the distributions of velocity and temperature as a function of the porosity parameter (λ^*)on both velocity and thermal profiles. When the value of $\lambda^*$is increased from 0.15 to 3.15, the velocity of THNF lowers. From a physical standpoint, the existence of porous material creates empty spaces inside the route of fluid flow, resulting in a stronger resistance force known as drag. As a result, the velocity of the fluid decreases. Moreover, the rising magnitude of λ^*leads to a simultaneous rise in the temperatureof the fluid and the thickness of the corresponding boundary layer(BL).

Effect of radiation parameter

The radiation parameter plays an important role in high-temperature industrial processes like gas turbines, combustion chambers, nuclear reactors, and solar thermal collectors.Figures 4 and 5 illustrate the influence of the radiation parameter on velocity and thermal distributions. The radiation parameter positively correlates with both velocity and temperature. Increasing the magnitude of R_d exposes the fluid molecules to more energy, resulting in increased speed and temperature levels.Momentum boundary layer thickness increases as momentum spreads more effectively due to enhanced energy**.** Thermal BL thickness also increase**s**, reflecting stronger thermal diffusion into the fluid.

Effect of dissipation parameter

The dissipation parameter is crucial in systems with significant viscous heating, such as micro-electrochemical systems, lubrication theory, or high-

speed aerospace flows.Figures 6 and 7 demonstrate the effect of the dissipation parameter on velocity and thermal profile. Increasing the dissipation parameter's magnitude results in an increase in both velocity and temperature. Physically, an increase in Ec indicates that the kinetic energy of fluid disturbances intensifies, leading to more frequent molecular collisions and the generation of heat, resulting in an increase in temperature.

Effect of thermal ratio parameter

The thermal ratio parameter, representing the wall-to-ambient temperature ratio, is particularly important in industrial coating, extrusion, and heat exchanger design.Figures 8 and 9 show the thermal ratio parameters (θ_S) effect on both velocity and thermal profile. As the valueof θ_S increases, the graph shows higher temperatures and velocities. An elevation in θ_S indicates that the surface temperature is greater than the temperature of the surrounding free-flowing air. In this scenario, the wall conveys a large amount of energy to the liquid located inside the boundary layer. As a result, both velocity and temperature increase. Consequently, both the momentum BL and the thermal BL expand in thickness, indicating a more significant influence of wall temperature on the fluid flow and HT.

Effect of slip parameter

The slip parameter is relevant in microfluidic devices, polymer extrusion, and biofluid transport, where velocity slip occurs due to surface roughness.Figures 10 and 11 show the effect of the slip parameter (ω) on the velocity and thermal profile. The computation of ω is carried out within a spectrum of 0.5 to 2.0. An increase in the value of the ω will lead to a decrease in the fluid's velocity. When a slip occurs (for non-zero values of ω), the velocity of the flow near the sheet is no longer the same as the velocity at which the sheet is stretching. This demonstrates that there is a velocity slip. Because of the slip phenomenon, the fluid only partially transmits the pulling force on the stretched sheet.This leads tothinner momentum BL, which is critical when designing systems with surface-sensitive flow behavior.

Effect of magnetic parameter

The magnetic parameter has strong relevance in magnetohydrodynamic generators, plasma flow control, and cooling of electronic components using liquid metals.Figures 12 and 13 show the variation of magnetic factors (M) on velocity and thermal profile. The computation of M is performed within the range of 0.01 to 4.01. The higher M value leads to a decrease in velocity profile and an increase in heat profile. A magnetic field generates the Lorentz force, which opposes the fluid's movement. This leads to a decrease in the velocity distribution and, therefore, a reduction in the BL of momentum.

Effect of variable thermal conductivity parameter

In systems involving smart fluids, phase-change materials, or nano-engineered composites, variable thermal conductivity is a key design factor.Figures 14 and 15 illustrate the impact of varying thermal conductivity (ε) on velocity and thermal profile. Thermal conductivity ε and velocity traces have a positive correlation, but the temperature traces exhibit an inverse association. These results demonstrate a fall in the momentum BL and an increase in the thermal BL.

Effect on SFC and LNN

Figures 16 and 17 depict the performance of SFC and LNN as they are sketched against ξ and ω parameters. These figures demonstrate that fluids encounter increased drag as slip parameter values increase, and the same trend holds for LNN. And, Figures 18 and 19 show that variations in Ec and R_d have a little effect on the drag force. However, when the Ec grows, the LNN decreases for all values of R_d.

Streamline and isothermal line discussion

Figure 20 shows the streamline patterns for presence/absence of the magnetic parameter. The left side indicate the absence of M, the streamlines are more dispersed and extend further into the fluid domain, signifying increased flow intensity and enhanced fluid circulation. The streamlines are well matched along the wall and progressively diverge, indicating improved momentum transmission in the boundary layer region.Upon the application of a magnetic field, the streamlines are compressed and concentrated adjacent to the surface. The flow intensity diminishes markedly, and the penetration depth of streamlines is diminished. This illustrates the dampening influence of the Lorentz force produced by the magnetic field.The influence of increasing thermal conductivity exhibits a contrary tendency. At Figure 21. lower value of $\omega = 0.45$ the streamlines are

restricted along the wall with minimal penetration, signifying diminished energy diffusion and the creation of a thinner boundary layer. As ω approaches 1.45, the streamlines extend outward and disperse over the fluid region, indicating intensified circulation and greater momentum transmission resulting from increased thermal diffusion. At a higher value of ω=2.45, the streamlines are extensively dispersed with enhanced curvature, signifying substantial heat diffusion and intensified buoyancy-driven flow, which increases the thickness of the boundary layer.The figures 22 and 23 given isothermal line plots demonstrate the impact of varying thermal conductivity ε and magnetic parameter M on the temperature distribution within the boundary layer. When the thermal conductivity increases (ε 0.45→1.45), the isothermal contours spread out further in the transverse direction (η). This shows that higher conductivity makes heat diffuse more quickly, which lowers temperature gradients along the wall. The magnetic parameter, on the other hand, has a negative effect on thermal transport. When M goes from 0.0 to 2.0, the isothermal lines move up and become denser. This is because the Lorentz force slows down the fluid motion, which thickens the thermal boundary layer and slows down the heat transfer rate.

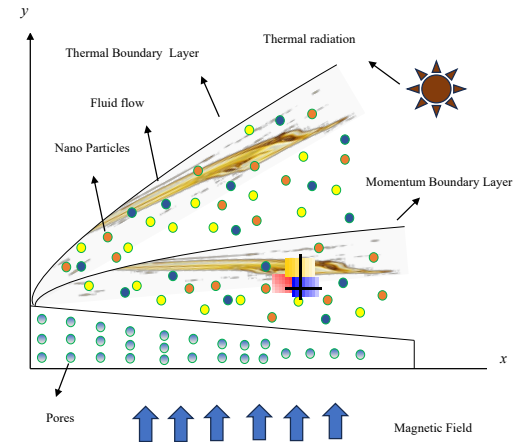

Fig 1. Physical model

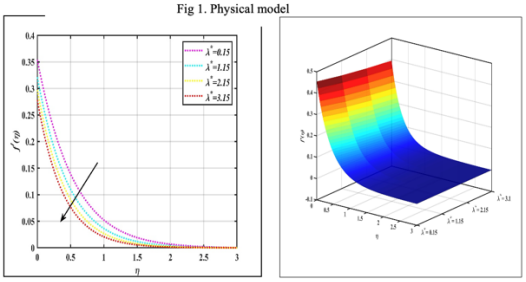

Fig 2.Influence of porosity on velocity profile.

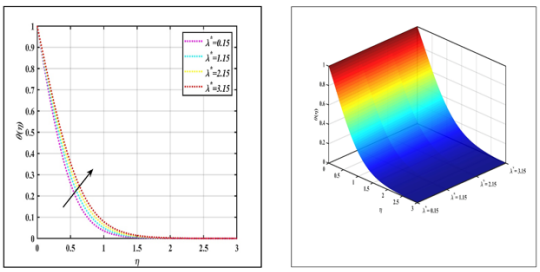

Fig 3.Influence of porosity on temperature profile.

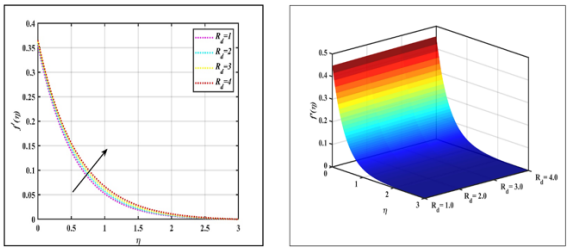

Fig 4.Influence of radiation parameter on velocity profile.

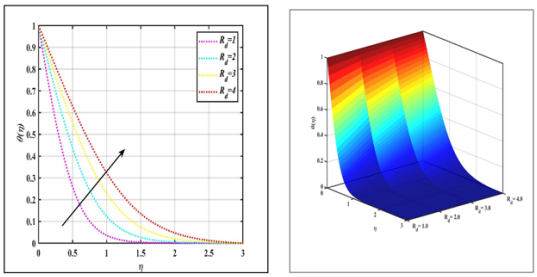

Fig 5.Influence of radiation parameter on temperature profile.

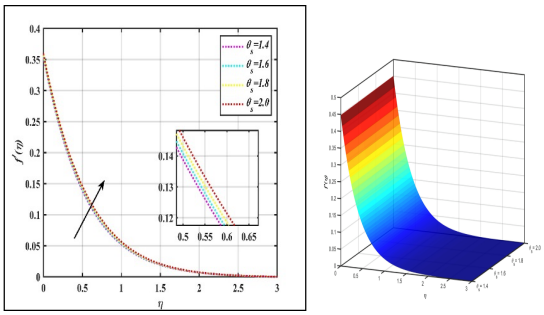

s

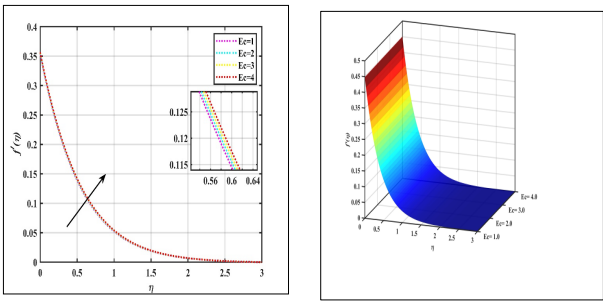

Fig 6. Influence of dissipation parameter on velocity profile.

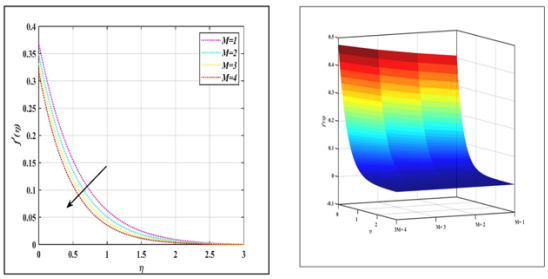

Fig 12.Influence of magnetic parameter on velocity profile.

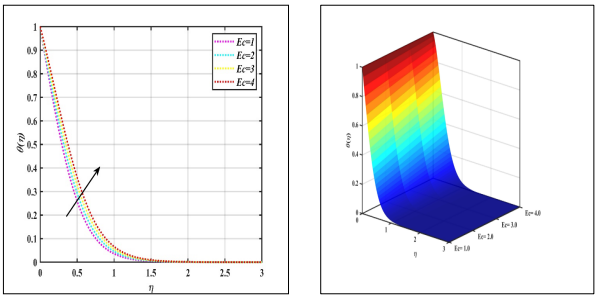

Fig 7.Influence of dissipation parameter on temperature profile.

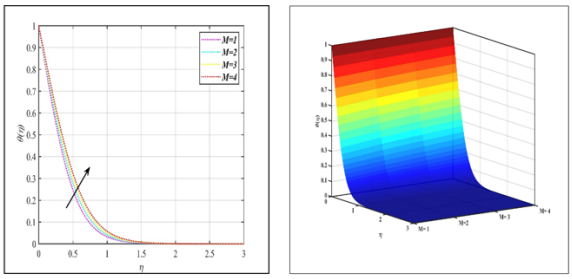

Fig 13.Influence of magnetic parameter on temperature profile.

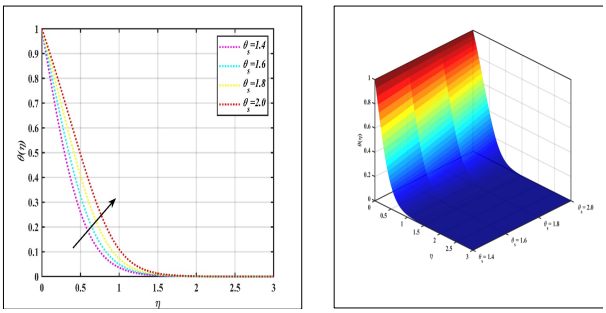

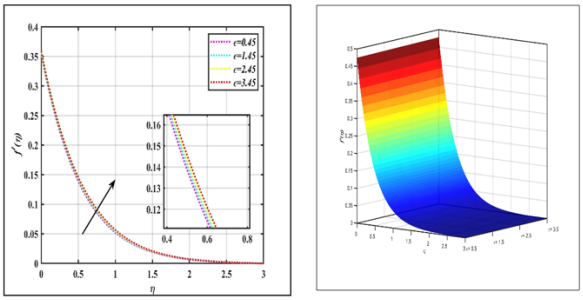

Fig 14.Influence of variable thermal conductivity on velocity profile.

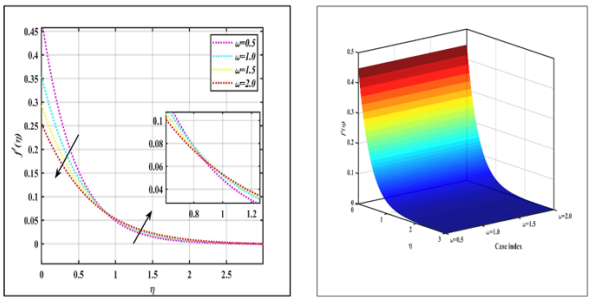

Fig 10.Influence of velocity slip parameter on velocity profile.

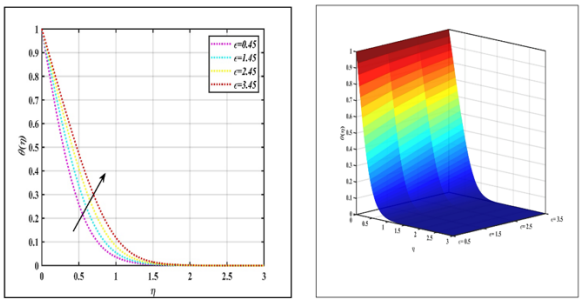

Fig 15.Influence of variable thermal conductivity on temperature profile.

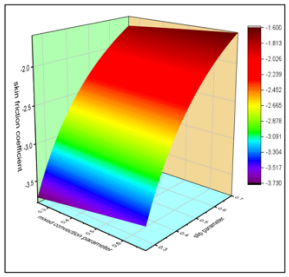

Fig 16.LSF radiation along dissipation parameter.

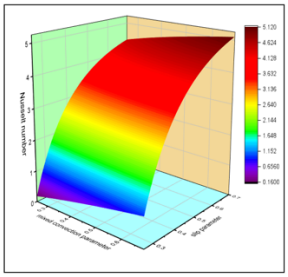

Fig 17.LNN radiation along dissipation parameter.

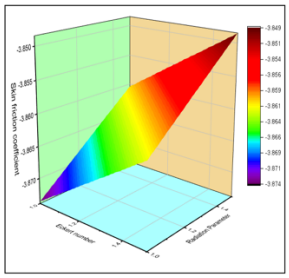

Fig 18.LSF radiation along dissipation parameter.

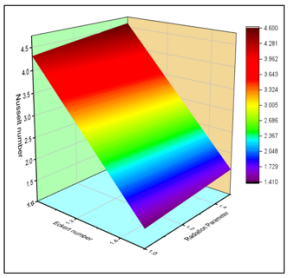

Fig 19. LNN radiation along dissipation parameter.

Conclusions

This paper presents a BVP4C solver-based numerical investigation to examine the flow characteristics of THNF flowing over a non-flat stretching sheet. The paper includes the following key findings:

- The growth in M favours the fluid's temperature while opposing fluid movement.
- Increasing λ^* results in a decline in fluid velocity; on the other hand, temperature rises.
- The thermal conductivity parameter directly relates to both fluid velocity and temperature.
- Growth in ω causes the fluid's temperature to rise, while the fluid's velocity exhibits dual behaviour.
- The magnitude of LNN increased by approximately 4.00% for a rise of one unit (2 to 3) in R_d, as observed from Table 4.
- We note a drop of around 10.80% in LNN with the variation in slip parameter from 1.5 to 2, as observed from Table 4.

Funding Information
No funding was received for this work.

Conflict of interest
No

Ethics declaration
Not applicable

Data availability statement
There is no data availability statement in this manuscript

References

1. Choi, S. U., & Eastman, J. A. (1995). Enhancing Thermal Conductivity of Fluids with Nanoparticles (Argonne, IL (United States): Argonne National Lab.(ANL)).
2. Xuan, Y., & Li, Q. (2000). Heat transfer enhancement of nanofluids. *International Journal of Heat and Fluid Flow*, *21*(1), 58-64.
3. Sridhara, V., & Satapathy, L. N. (2015). Effect of nanoparticles on thermal properties enhancement in different oils–a review. *Critical Reviews in Solid State and Materials Sciences*, *40*(6), 399-424.
4. Tiwari RK, Das MK.(2007) Heat transfer augmentation in a two-sided lid-driven differentially heated square cavity utilizing nanofluids.*International Journal ofHeat and Mass Transfer* 50(9-10), 2002–2018.
5. Shima, P. D., & Philip, J. (2014). Role of thermal conductivity of dispersed nanoparticles on heat transfer properties of nanofl
Chemistry Research, 55(2), 980-988.
6. Zahmatkesh, I., Sheremet, M., Yang, L., Heris, S. Z., Sharifpur, M., Meyer, J. P., Ghalambaz, M., Wongwises, S., &Mahian, O.

(2021). Effect of nanoparticle shape on the performance of thermal systems utilizing nanofluids: A critical review. *Journal of Molecular Liquids*, *321*, 114430.

7. Tang, Z., Zhao, J., Wang, Y., & Liu, Z. (2023). Understanding the role of nanoparticles in boiling phase transition: The effect of nanoparticle shape. *Journal of Molecular Liquids*, *371*, 121110.
8. Buongiorno, J. (2006). Convective transport in nanofluids, 128, 240-250. DOI: 10.1115/1.2150834.
9. Cheng, L. (2009). Nanofluid heat transfer technologies. *Recent Patents on Engineering*, *3*(1), 1-7.
10. Devi, S. U., & Devi, S. A. (2017). Heat transfer enhancement of Cu−Al_2O_3water hybrid nanofluid flow over a stretching sheet. *Journal of the Nigerian Mathematical Society*, *36*(2), 419-433.
11. Sheikholeslami, M. (2022). Numerical investigation of solar system equipped with innovative turbulator and hybrid nanofluid. *Solar Energy Materials and Solar Cells*, *243*, 111786.
12. Bhatti, M. M., Ellahi, R., & Doranehgard, M. H. (2022). Numerical study on the hybrid nanofluid (Co_3O_4-Go/H_2O) flow over a circular elastic surface with non-Darcy medium: Application in solar energy. *Journal of Molecular Liquids*, *361*, 119655.
13. Gupta, T., Pandey, A. K., & Kumar, M. (2024). Numerical study for temperature-dependent viscosity based unsteady flow of GP-MoS_2/$C_2H_6O_2$-H_2O over a porous stretching sheet. *Numerical Heat Transfer, Part A: Applications*, *85*(7), 1063-1084.
14. Xia, W. F., Ahmad, S., Khan, M. N., Ahmad, H., Rehman, A., Baili, J., & Gia, T. N. (2022). Heat and mass transfer analysis of nonlinear mixed convective hybrid nanofluid flow with multiple slip boundary conditions. *Case Studies inThermal Engineering*, *32*, 101893.
15. Shoeibi, S., Kargarsharifabad, H., Rahbar, N., Ahmadi, G., & Safaei, M. R. (2022). Performance evaluation of a solar still using hybrid nanofluid glass cooling-CFD simulation and environmental analysis. *Sustainable Energy Technologies and Assessments*, *49*, 101728.
16. Puneeth, V., Manjunatha, S., Madhukesh, J. K., & Ramesh, G.K. (2021). Three dimensional mixed convection flow of hybrid Casson nanofluid past a non-linear stretching surface: A modified Buongiorno's model aspect. *Chaos, Solitons & Fractals*, *152*, 111428.
17. Yaseen, M., Rawat, S.K., & Kumar, M. (2022). Cattaneo–Christov heat flux model in Darcy–Forchheimer radiative flow of MoS_2–SiO_2/kerosene oil between two parallel rotating disks. *Journal of Thermal Analysis and Calorimetry*, *147*(19), 10865-10887.
18. Sahoo, R. R., & Kumar, V. (2020). Development of a new correlation to determine the viscosity of ternary hybrid nanofluid. *International Communications in Heat and Mass Transfer*, *111*, 104451.